Wind and Structures, *Vol. 28, No. 2 (2019) 111-128*
DOI: https://doi.org/10.12989/was.2019.28.2.111

An efficient optimization approach for wind interference effect on octagonal tall building

Rony Kar[a], Sujit Kumar Dalui* and Soumya Bhattacharjya[b]

Department of Civil Engineering, Indian Institute of Engineering Science and Technology, Shibpur, Howrah – 711103, India

(Received January 25, 2018, Revised September 14, 2018, Accepted October 13, 2018)

Abstract. In this paper an octagon plan shaped building (study building) in presence of three square plan shaped building is subjected to boundary layer wind flow and the interference effects on the study building is investigated using Computational fluid dynamics. The variation of the pressure coefficients on different faces of the octagon building is studied both in isolated and interference conditions. Interference Factors (IF) are calculated for different faces of the study building which can be a powerful tool for designing similar plan shaped buildings in similar conditions. A metamodel of the IF, in terms of the distances among buildings is also established using Response Surface Method (RSM). This set of equations are optimized to get the optimum values of the distances where the IF is unity. An upstream Interference zone for this building setup and wind environment is established from these data. Uncertainty principle is also utilised to determine the optimum positions of the interfering buildings considering the uncertain nature of wind flow for minimum interference effect. The proposed procedure is observed to be computationally efficient in deciding optimum layout at buildings often required in city planning. The results show that the proposed RSM-based optimization approach captures the interference zone accurately with substantially less number of experiments.

Keywords: computational fluid dynamics; interference factor; interference zone; optimization; pressure coefficient; response surface method; tall building

1. Introduction

With the increasing population throughout the world it is now an absolute necessity to construct tall and super-tall structures for accommodation as well as for entertainment purpose. As the height of the building increases it becomes more vulnerable to wind as compared to earthquake. So, wind engineering has become a subject of utmost importance in the field of structural engineering to analyse and enumerate the effect of wind, on a standalone structure or interference of other structures on it, in natural or built environment. A significant amount of research has been conducted in this field by extensive experimentation as well as different analytical methods. There have been optimization studies as well on tall buildings subjected to wind load. Spence and Gioffrè (2012) performed reliability-based design optimization of wind excited building. Venanzi and Materazzi (2013) presented optimization of a hybrid control system for wind-exposed tall buildings with uncertain mass distribution. Wu *et al.* (2016) presented optimization of tall structure under wind load excitation and conducted experimental study of a wind resistant bearing. But, these researches did not consider any interference effect. However, like seismic pounding effect, or pile to pile interaction, there is significant impact of mutual interference effect of wind load as well on tall buildings. Thus, in recent past wind interference effect is gaining attention among the researchers. Most of the researches on wind interference effect is conducted on the study building in presence of only one interfering building (e.g., Yu *et al*. 2015, Zhang and Gu 2008). Both wind tunnel experiments and CFD have been employed in various works to find out the effect of interference on pressure coefficients. Wang *et al.* (2014) investigated the interference effects of a neighbouring building on wind loads on scaffolding of a rectangular plan shaped building. A few researches have been conducted (Lo *et al*. 2017, Yan and Li 2016) to observe and quantify the wind interference effect on different aerodynamically modified tall buildings with various interfering arrangements. Lo *et al.* (2016) calculated the wind interference effect on twin supertall buildings in different interfering arrangements by comparing force coefficients, buffeting factor and response trajectories. Hui *et al.* (2012), Hui *et al.* (2013) and Mara *et al.* (2014) conducted wind tunnel tests for finding out the interference effect on local peak pressure coefficients on regular plan shaped (square and rectangular) buildings. Pressure and flow field investigation has been carried out by Hui *et al.* (2013) to find out the interference effect on peak pressure for two square and rectangular plan shaped buildings in interfering condition. Zu and Lam (2018) carried out wind tunnel tests to investigate the effect of mutual interference on along wind and across wind dynamic behaviour of twin tall buildings. Among other notable research works, interference effect on wind induced torsional moment of rectangular and square plan shaped building (Hui *et al.* 2017, Yu *et al*. 2016) has also been carried out. Lam *et al.*

*Corresponding author, Assistant Professor
E-mail: sujit_dalui@rediffmail.com
[a] Ph.D. Student
[b] Assistant Professor

ISSN: 1226-6116 (Print), 1598-6225 (Online)

(2008) and Lam *et al.* (2011) conducted wind tunnel tests and CFD analyses on a row of five square plan shaped tall buildings to find out the static and dynamic response the buildings in different interference condition. Hang *et al.* (2011) studied experimentally and numerically the flow characteristics through high-rise square building arrays of different packing density. Thus, the present study explores wind interference effect of tall buildings. Particularly, the object of the study is to obtain an efficient procedure so that the building layout planning of a city can be optimally decided to have minimum adverse wind interference effect. Generally, wind load is assessed in a building considering it as stand-alone. However, as explained, there may be adverse effect of wind interference on the main study building taken for design. Thus, if one wants to minimize these adverse interference effect, right in the planning stage of a city, the city buildings will be safe from large adverse wind interference effect. In doing so, a numerical study composed of three interfering buildings and one study building will be presented. The procedure, being generic in nature, can be extended to multiple number of interfering buildings with different aspect ratio and plan ratio.

The wind interference is conventionally measured in terms of Interference factor (IF), which vary significantly with distance from the adjacent building, aspect ratio, plan ratio and shape of study building. Keeping this in view, the IF is minimized in this study using Broyden–Fletcher–Goldfarb–Shanno (BFGS) Quasi-Newton method with a cubic line search procedure. This method requires explicit functional form of IF. But, IF is implicit with respect to the influencing parameters. Hence, a Response Surface Method (RSM) based metamodels has been adopted in the present study to approximate IF in terms of the influencing parameters. Moreover, if one wants to carry out the same study by random trial instead of using RSM, prohibitively large experiments will be required. It may be noted here that the application of RSM based optimization approach in the field of wind engineering is very scarce, especially in context of behaviour of tall structures due to wind. Bhandari (2018) presented wind fragility analysis of tall building using RSM based metamodels. In fact, there are only few studies dealing with optimization of structure in RSM framework considering wind, e.g., helicopter rotor for low vibration (Ganguli 2002), wind turbine air foils (Li *et al.* 2010). But, studies addressing wind interference effect on tall building in RSM framework has not yet been observed in the existing literature and builds the uniqueness of this study.

RSM is used to cast the relationship among dependent and independent variables in the form of explicit equations, which is useful for calculating the sensitivity gradient. In the current research the optimization approach in conjunction with uncertainty principle is applied to depict the interference zone for the building setup. This RSM based metamodelling approach can potentially be extrapolated for more number of buildings with different plan shape, aspect ratio and various wind incidence angles, which in turn can cover the wind engineering aspect for a prospective planning of a city.

It has been realized that wind effect on tall building has several sources of uncertainty such as wind speed, wind incidence angle, possible location of interfering building (Venanzi and Materazzi 2013, Bhandari *et al.* 2018). Thus, an attempt has been made to incorporate uncertainty in the optimization process. The location of the building is considered uncertain up to some extent. However, there is no definite probability distribution function available which represents this uncertainty. Only, the possible range of variation may be known to a town planner. Thus, the uncertainty in building location is considered to be uncertain-but-bounded type, which is governed by interval analysis. In presence of uncertainty, IF may vary to unfavourable side, which is duly considered in this study by optimizing the worst possible value of IF.

Despite abundance of various researches in the field of wind engineering with respect to the shape of study building, very few analyses have been carried out on the octagon plan shaped building. Among its various advantages, the most obvious one is that an octagon plan shaped building encompasses 20% more plan area than its square counterpart of same perimeter, which in itself is of massive significance in this age of aggressive urbanization. The octagonal plan shape can also be considered as a particular case of square building with chamfered corners for better aerodynamic response. Moreover, it is evident from the past research works, most of the studies on interference have been carried out on square or rectangular plan shaped buildings and only for two buildings disregarding a very few exceptions (Lam *et al.* 2008, Lam *et al.* 2011). In this paper the octagonal plan shaped study building, in presence of three interfering buildings, is analysed and pressure coefficients as well as IF for different positions of the interfering buildings are found out. The results of the proposed RSM based optimization study of wind interference problem will be validated by numerical simulation by computational fluid dynamics (CFD).

Thus, the objectives and unique contributions of this study in a nutshell are: i) to propose a procedure for optimal layout planning of buildings considering wind interference effect, ii) to explore RSM in such optimization to make the procedure computationally viable, iii) to incorporate uncertainty in this optimization study of wind interference problem, and iv) validation of the proposed RSM based procedure by a CFD analysis. In doing so, the octagonal plan shaped building is taken up since it is less focused in the existing literature despite of several advantage of such building shape.

2. Numerical analysis by CFD

The octagon and square plan shaped buildings in both isolated and interference condition are analysed with the help of CFX module in ANSYS v18.1. Atmospheric Boundary Layer (ABL) wind profile is used which is governed by the power law equation

$$U(z) = U_\infty \left(\frac{z}{z_0}\right)^\alpha \tag{1}$$

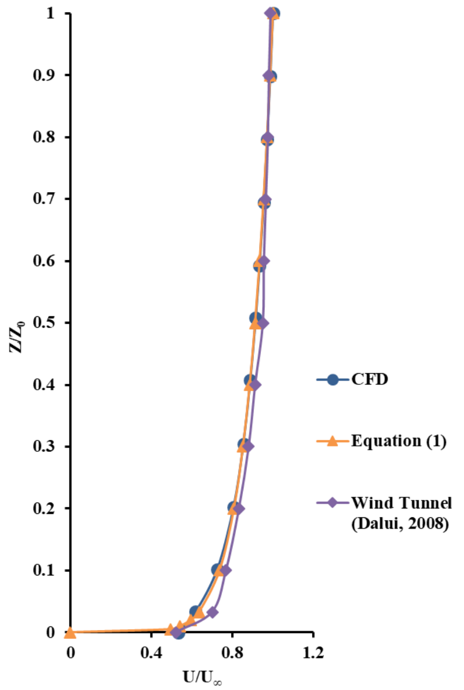

(a)

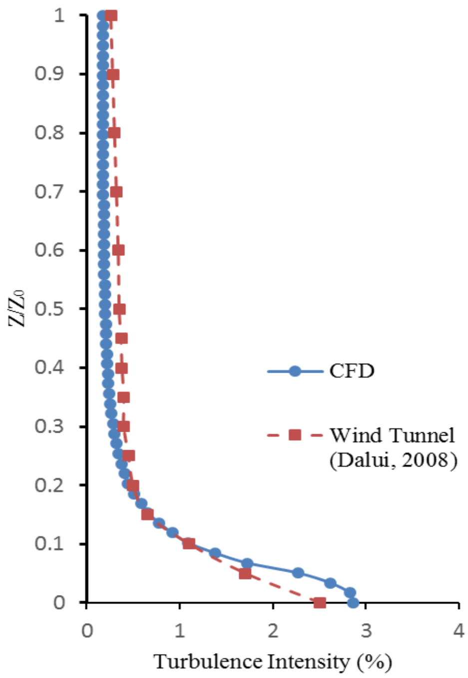

(b)

Fig. 1 Comparison of (a) ABL velocity profile and (b) Turbulence Intensity by different methods

Where, z = Height at any point, z_0 = Boundary layer height, U∞= Free stream velocity, U(z) = Velocity at height 'z'. The power law exponent α=0.133 is used which corresponds to terrain category II in IS 875-part III (2015).

The velocity profile generated by CFD is compared with the profile derived from equation (1) and the wind tunnel data used in Ph.D. thesis by Dalui (2008) in Fig. 1(a). Whereas Fig. 1(b) shows the comparison between Turbulence Intensity variations simulated by CFD and extracted from wind tunnel data. It can be observed that the velocity profiles and the Turbulence Intensity profiles from the CFD analysis and wind tunnel experiment matches with satisfactory accuracy due to utilisation of similar wind environment in both cases. Hence, it can be stated that the flow characteristics for both the cases are almost identical as expected.

2.1 Details of turbulence model

All the buildings are modelled in 1:300 length scale and wind velocity is taken as 50 m/s. Mainly k-ε model is used for the numerical solution. Apart from that SST and k-ω models are also used to compare the results with that from k-ε model.

2.1.1 k-ε model

As stated in Kar and Dalui (2016), the k-ε models use the gradient diffusion hypothesis to relate the Reynolds stresses to the mean velocity gradients and the turbulent viscosity. The turbulent viscosity is modelled as the product of a turbulent velocity and turbulent length scale. k is the turbulence kinetic energy and is defined as the variance of the fluctuations in velocity. It has dimensions of (L2T-2). ε is the turbulence eddy dissipation and has dimensions of per unit time. The continuity equation and momentum equations are

$$\frac{\partial \rho}{\partial t} + \frac{\partial}{\partial x_j}(\rho U_j) = 0 \tag{2}$$

$$\frac{\partial \rho U_i}{\partial t} + \frac{\partial}{\partial xj}(\rho U_i U_j) = -\frac{\partial p'}{\partial x_i} + \frac{\partial}{\partial x_j}\left[\mu_{eff}\left(\frac{\partial U_i}{\partial x_j} + \frac{\partial U_j}{\partial x_i}\right)\right] + S_M \tag{3}$$

Where S_M is the sum of body forces, μ_{eff} is the effective viscosity accounting for turbulence, and p' is the modified pressure. ρ and U denote density and velocity respectively. The k-ε model is based on the eddy viscosity concept, so that

$$\mu_{eff} = \mu + \mu_t \tag{4}$$

μ_t is the turbulence viscosity

$$\mu_t = C_\mu \rho \frac{k^2}{\varepsilon} \tag{5}$$

The values of k and ε come directly from the differential transport equations for the turbulence kinetic energy and turbulence dissipation rate

$$\frac{\partial(\rho k)}{\partial t} + \frac{\partial}{\partial x_j}(\rho k U_j) = \frac{\partial}{\partial x_j}\left[\left(\mu + \frac{\mu_t}{\sigma_k}\right)\frac{\partial k}{\partial x_j}\right] + P_k + P_b - \rho\varepsilon - Y_M + S_k \tag{6}$$

$$\frac{\partial(\rho \mathcal{E})}{\partial t} + \frac{\partial}{\partial x_j}(\rho \varepsilon U_j) = \frac{\partial}{\partial x_j}\left[\left(\mu + \frac{\mu_t}{\sigma_\varepsilon}\right)\frac{\partial \mathcal{E}}{\partial x_j}\right] + \rho C_1 S_\varepsilon - \rho C_2 \frac{\mathcal{E}^2}{k + \sqrt{\nu \mathcal{E}}} + C_{1\varepsilon}\frac{\mathcal{E}}{k} C_{3\varepsilon} P_b + S_\varepsilon \quad (7)$$

Pk represents the generation of turbulence kinetic energy due to the mean velocity gradients, Pb is the generation of turbulence kinetic energy due to buoyancy and Ym represents the contribution of the fluctuating dilatation in compressible turbulence to the overall dissipation rate, C1 and C2 are constants. σk and σε are the turbulent Prandtl numbers for k (turbulence kinetic energy) and ε (dissipation rate). The values considered for C1ε, σk and σε are 1.44, 1 and 1.2 respectively.

2.2 Domain and meshing

A domain is constructed as recommended by Franke *et al*. (2004) which has 5H upwind fetch, 15H downwind fetch and 5H top and side clearances, where 'H' is the height of the model. The aforementioned domain for study building in isolated condition is shown in Fig. 2(a) and for interfering condition in Fig. 2(b). The clearances are taken from the building (study building or interfering building) nearest to the domain boundary in each case. The domain is constructed so that the flow of the wind is not restricted and all the characteristic behaviours of wind can be observed. No blockage correction is needed for this domain. The domain and the building meshing is done using tetrahedral elements (Lo *et al*. 2016).

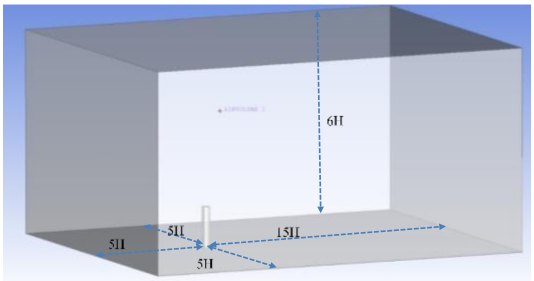

(a) Isolated Condition

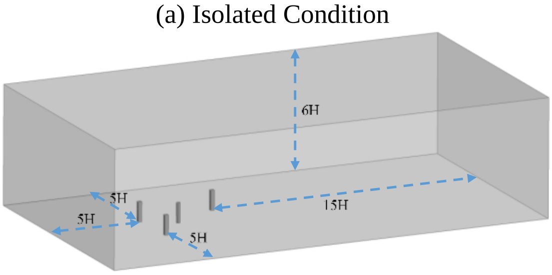

(b) Typical interfering condition

Fig. 2 Computational domain for study building used for CFD simulation for different cases

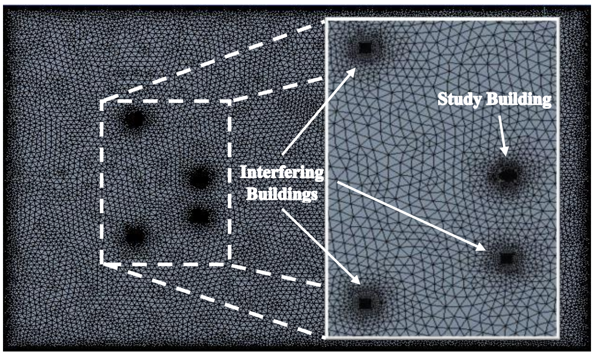

Fig. 3 Meshing of the domain and its zoom in view for a typical interfering case

The meshing elements near the building setup is smaller than that in the rest of the domain to accurately analyse the higher gradient region of the wind flow. No slip wall is considered for the building faces and the floor of the domain, whereas free slip wall is provided elsewhere. The analysis is done under atmospheric pressure (1 atm= 101325 Pa). Reynolds Numbers of the models are in the order of ~106. Low turbulence intensity is provided at the inlet as well as in the domain. The meshing in a typical interference case is shown in Fig. 3.

3. Parametric study

The actual heights of the buildings are 150 m and the diameter of the circle inscribed in the plan shape is 30 m for both the study octagon plan shaped object building and square plan shaped interfering buildings. The buildings are modelled in 1:300 scale for analysis. The scaled down height of the buildings is 500 mm and the scaled down diameter of the circle inscribed in the plan shape is 100 mm for all the buildings. The aspect ratio is 1:5 for the study building as well as interfering buildings. The building setup to be analysed for typical interfering case is shown in Fig. 4 for 0° wind incidence angle only. The spacing from the study building to upstream interfering buildings is S1, the spacing between the upstream interfering buildings is S2 and the spacing between the study and the third interfering building is S3. The interfering cases which are to be analysed by ANSYS CFX are described in Table 1.

Table 1 Description of different Interfering cases

Cases	Spacing between buildings		
	S_1 (mm)	S_3 (mm)	S_2 (mm)
Case I	200	200	200, 300, 500…10000
Case II	200	300	200, 300, 500…10000
Case III	200	500	200, 300, 500…10000
Case IV	200	750	200, 300, 500…10000
Case V	200	1000	200, 300, 500…10000

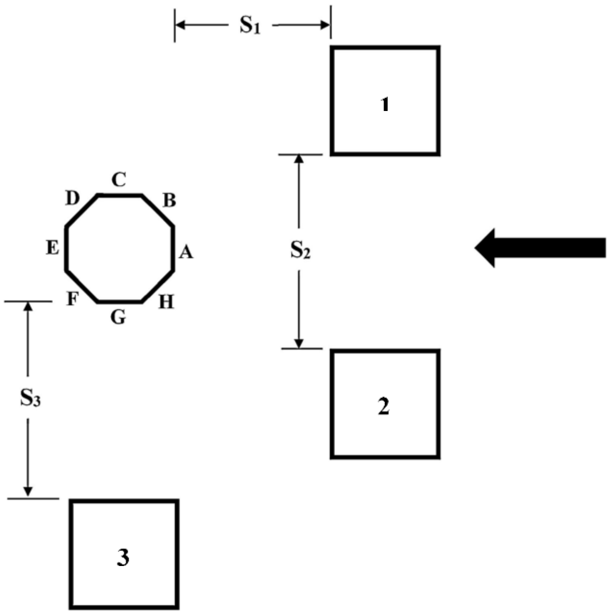

Fig. 4 Plan of study building and interfering building with wind flow direction

4. Numerical modelling by RSM and optimization

The RSM as described by Myers and Montgomery (2009) is used to construct an empirical model of the IFs with the input variables being S_1, S_2 and S_3. Uniform design method with type III polynomial is used as the Design of Experiments (DoE). The model may be cast in the form.

$$Y^{\langle i\rangle} = \beta_0^{\langle i\rangle} + \sum_{j=1}^{k} \beta_j^{\langle i\rangle} x_j + \sum_{jj=1}^{k} \beta_{jj}^{\langle i\rangle} x_{jj}^2 \qquad (8)$$

$$i = 1, 2, 3, \ldots, n$$

Where k= Number of input variables, n= Number of data points. Thus for ‘n’ data points

$$\begin{bmatrix} 1 & x_{11} & x_{12} & \cdots & x_{1k} & x_{11}^2 & x_{12}^2 & \cdots & x_{1k}^2 \\ 1 & x_{21} & x_{22} & \cdots & x_{2k} & x_{21}^2 & x_{22}^2 & \cdots & x_{2k}^2 \\ \vdots & \vdots & \vdots & \ddots & \vdots & \vdots & \vdots & \ddots & \vdots \\ 1 & x_{n1} & x_{n1} & \cdots & x_{nk} & x_{n1}^2 & x_{n2}^2 & \cdots & x_{nk}^2 \end{bmatrix} \begin{Bmatrix} \beta_0 \\ \beta_1 \\ \vdots \\ \beta_n \end{Bmatrix} = \begin{Bmatrix} Y_{\langle 0\rangle} \\ Y_{\langle 1\rangle} \\ \vdots \\ Y_{\langle n\rangle} \end{Bmatrix} \qquad (9)$$

Which can be written in matrix form as

$$\mathbf{X\beta} = \mathbf{Y} \qquad (10)$$

$$\text{Or,} \quad \boldsymbol{\beta} = (\mathbf{X}^{\mathrm{T}}\mathbf{X})^{-1}\mathbf{X}^{\mathrm{T}}\mathbf{Y} \qquad (11)$$

Where **X** is the design matrix, **β** is the coefficient vector and **Y** is the output vector. From Eq. (11) **β** can be calculated from which in turn the expressions for **Y** can also be found. This set of equations are optimized to unity and the different sets of $[S_1\ S_2\ S_3]^T$ are suggested for which the IFs on all the faces of the study building (octagon plan shaped) are unity, i.e., the study building behaves as that in isolated condition. Now the problem can be framed as the minimization problem for the objective function $f_i(\mathbf{S})$, i=1, 2…8 where $\mathbf{S}= [S_1\ S_2\ S_3]^T$, i.e.

$$\text{Minimize,} \ f_i(\boldsymbol{S}) = Y^{\langle i\rangle}(\boldsymbol{S}) - Y^t \qquad (12)$$

Where Y^t is the target interference factor taken as unity. $Y^{\langle i\rangle}$ is the IF at the i^{th} face. The problem becomes an unconstrained multidimensional multi-objective optimization problem which may be conveniently expressed as

$$\Psi(\boldsymbol{S}) = [f_1(S)\ f_2(S) \ldots f_8(S)] \qquad (13)$$

The solution of such problem can be done by the Evolutionary Algorithm, the Weighted-Sum Method, the particle swarm optimization etc. Owing to the simplicity and less computational time requirement the weighted sum method (WSM) has been adopted in the present study. Thus, by the WSM, the desirability function becomes

$$\Phi(\boldsymbol{S}) = \sum_{i=1}^{8} w_i\, f_i(\boldsymbol{S}) \qquad (14)$$

Where w_i is the weight factor for $f_i(\boldsymbol{S})$ and taken as 0.125 considering equal weight on each IF.

5. Incorporation of uncertainty in optimization technique

Wind load is very uncertain in nature. It is very difficult and cumbersome process to generate a wind environment which incorporates every aspect of uncertainty that a natural wind environment displays. So, in this case the effect of uncertainty is indirectly incorporated in the analysis by modifying the position of the interfering buildings, i.e., introducing uncertainty in the distances S_1, S_2 and S_3. The **S** is considered to be uncertain but bounded type (Bhattacharjya and chakraborty 2011) with defined lower and upper bound but no probability density function.

$$\Delta x_{ik} = u_k \times x_i \qquad (15)$$

Since, this paper uses perturbation theory based on first order Taylor series expansion (FOTSE) about the mean value (x_i), the uncertainty level (u_k) is taken as 15%. There is a chance that u_k may vary more than 15%. But, in such case FOTSE will not be valid and one may apply convex programming based non-probabilistic approach of optimization under uncertainty (Chen *et al.* 2017). This requires a detailed study and thus remains beyond the scope of this study.

Using First order Taylor series expansion about x_i one can derive the range of variation of $Y^{\langle i\rangle}$ due to uncertainty as

$$\Delta Y^{i\langle m\rangle} = \left[\frac{\partial Y^{\langle i\rangle}}{\partial x_1}\ \frac{\partial Y^{\langle i\rangle}}{\partial x_2} \cdots\right]^T \begin{Bmatrix} \Delta x_{1k} \\ \Delta x_{2k} \\ \vdots \end{Bmatrix} = \sum_{j=1}^{k} \left|\frac{\partial Y^{\langle i\rangle}}{\partial x_{ij}}\right| \Delta x_{ik} \qquad (16)$$

Similarly, nominal value of $Y^{\langle i\rangle}$ is

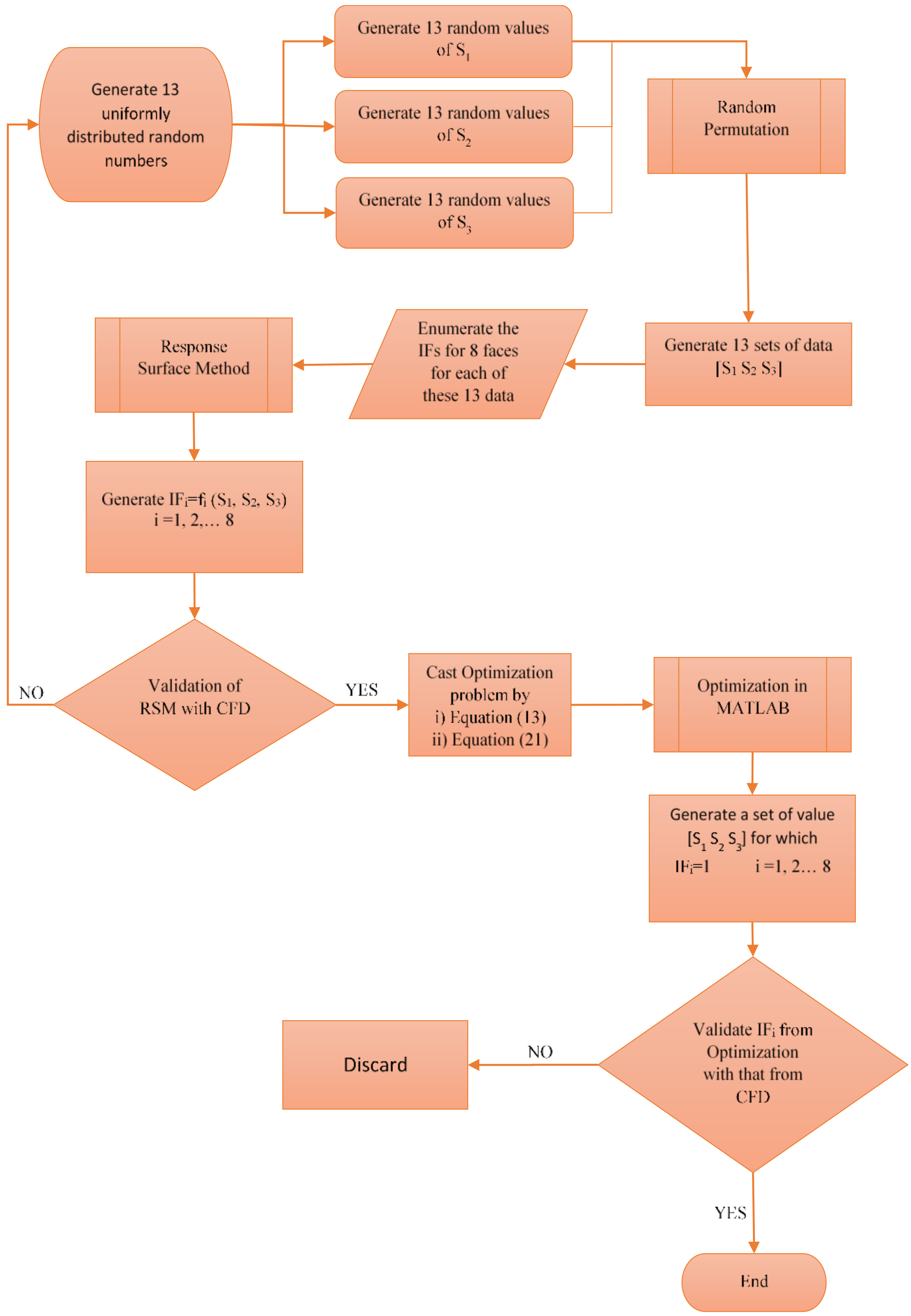

Fig. 5 Process for the analysis by RSM and Optimization

$$\overline{Y}^{\langle i \rangle, m} = Y^{\langle i \rangle} \pm \Delta Y^{\langle i \rangle, m} \tag{17}$$

It may be noted that, $Y^{\langle i \rangle}$ does not incorporate uncertainty and $\overline{Y}^{\langle m \rangle}$ takes uncertainty effect into account. The modified objective function $\overline{\Phi}^{\langle m \rangle}(\mathbf{S})$ can be found out by replacing $Y^{\langle i \rangle}$ with $\overline{Y}^{\langle i \rangle, m}$ as

$$\text{To minimize} \quad \overline{\Phi}^{\langle m \rangle}(\mathbf{S}) = \sum_{i=1}^{8} w_i \, \overline{f_i}^{\langle m \rangle}(\mathbf{S}) \tag{18}$$

$$\text{where} \quad \overline{f_i}^{\langle m \rangle}(\mathbf{S}) = Y^{\langle m \rangle}(\mathbf{S}) - Y^t \tag{19}$$

Thus, the problem becomes minimization problem of

$$\Psi^{\langle m \rangle}(\mathbf{S}) = [\overline{f_1}^{\langle m \rangle}(S)\ \overline{f_2}^{\langle m \rangle}(S) \ \dots \ \overline{f_3}^{\langle m \rangle}(S)] \tag{20}$$

The flow chart of the whole procedure is shown in Fig. 5.

Table 2 Comparison of face average values of pressure coefficient for square plan shaped building

Wind loading Code/Software Package		Face-A	Face-B	Face-C	Face-D
ANSYS CFX	k-ε	0.83	-0.47	-0.6	-0.6
	SST	0.84	-0.51	-0.63	-0.63
AS/NZS-1170.2 (2011)		0.80	-0.50	-0.65	-0.65
Deviation of ANSYS CFX wrt AS/NZS-1170.2 (2011)	k-ε	+3.75%	+6.0%	+7.7%	+7.7%
	SST	+5.0%	-2.0%	+4.62%	+4.62%
ASCE 7-10 (2010)		0.80	-0.50	-0.70	-0.70
Deviation of ANSYS CFX wrt ASCE 7-10 (2010)	k-ε	+3.75%	+6.0%	+14.3%	+14.3%
	SST	+5.0%	-2.0%	+10.0%	+10.0%
IS 875 part 3 (2015)		0.80	-0.25	-0.80	-0.80
Deviation of ANSYS CFX wrt IS 875 part 3 (2015)	k-ε	+3.75%	+88.0%	+25.0%	+25.0%
	SST	+5.0%	+104.0%	+21.25%	+21.25%

Table 3 Comparison of force coefficients for octagon plan shaped building

Wind loading Code/ Software Package		Force Coefficient
ANSYS CFX	k-ε	1.18
	SST	1.21
AS/NZS-1170.2 (2011)		1.40
Deviation of ANSYS CFX wrt AS/NZS-1170.2 (2011)	k-ε	-15.7%
	SST	-13.6%
ASCE 7-10 (2010)		1.14
Deviation of ANSYS CFX wrt ASCE 7-10 (2010)	k-ε	+3.5%
	SST	-6.1%
IS 875 part 3 (2015)		1.2
Deviation of ANSYS CFX wrt IS 875 part 3 (2015)	k-ε	-1.7%
	SST	+0.8%
Experimental Result (PhD thesis by Dalui 2008)		1.23
Deviation of ANSYS CFX wrt PhD thesis	k-ε	-4.1%
	SST	-1.6%

6. Results and discussion

6.1 Simulation by ANSYS CFX

Numerical simulation is carried out to investigate the pressure distribution on various surfaces of octagon plan shaped building for both isolated condition and interference condition.

6.1.1 Isolated condition

In this case both the interfering building and the study building are analysed in isolated condition separately.

<u>Square building</u>

The square building in isolated condition is analysed, in the aforementioned domain with k-ε and SST turbulence models, under the previously discussed wind environment for 0° wind angle. The face average values of the coefficients of pressure are calculated from the ANSYS CFX package and compared with that from wind action codes of different countries in Table 2.

In this case the deviation of the values derived from ANSYS CFX from AS/NZS-1170.2 (2011) is within acceptable limit. Variation exists in other cases due difference in the wind environment and method adopted.

<u>Octagon building</u>

The object building, i.e., the octagon plan shaped building is subjected to wind at 0° incidence angle and analysed by ANSYS CFX using k-ε turbulence model. The force coefficient of the octagon plan shaped building is enumerated using ANSYS CFX package and compared with that from wind action codes from different countries as well as experimental result in Table 3.

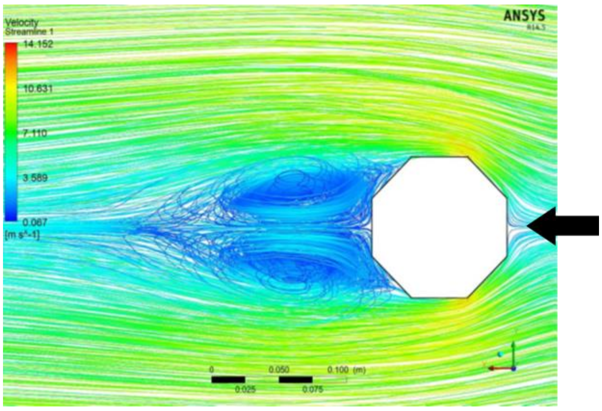

Fig. 6 Wind flow pattern around isolated octagon plan shaped building for 0° wind angle

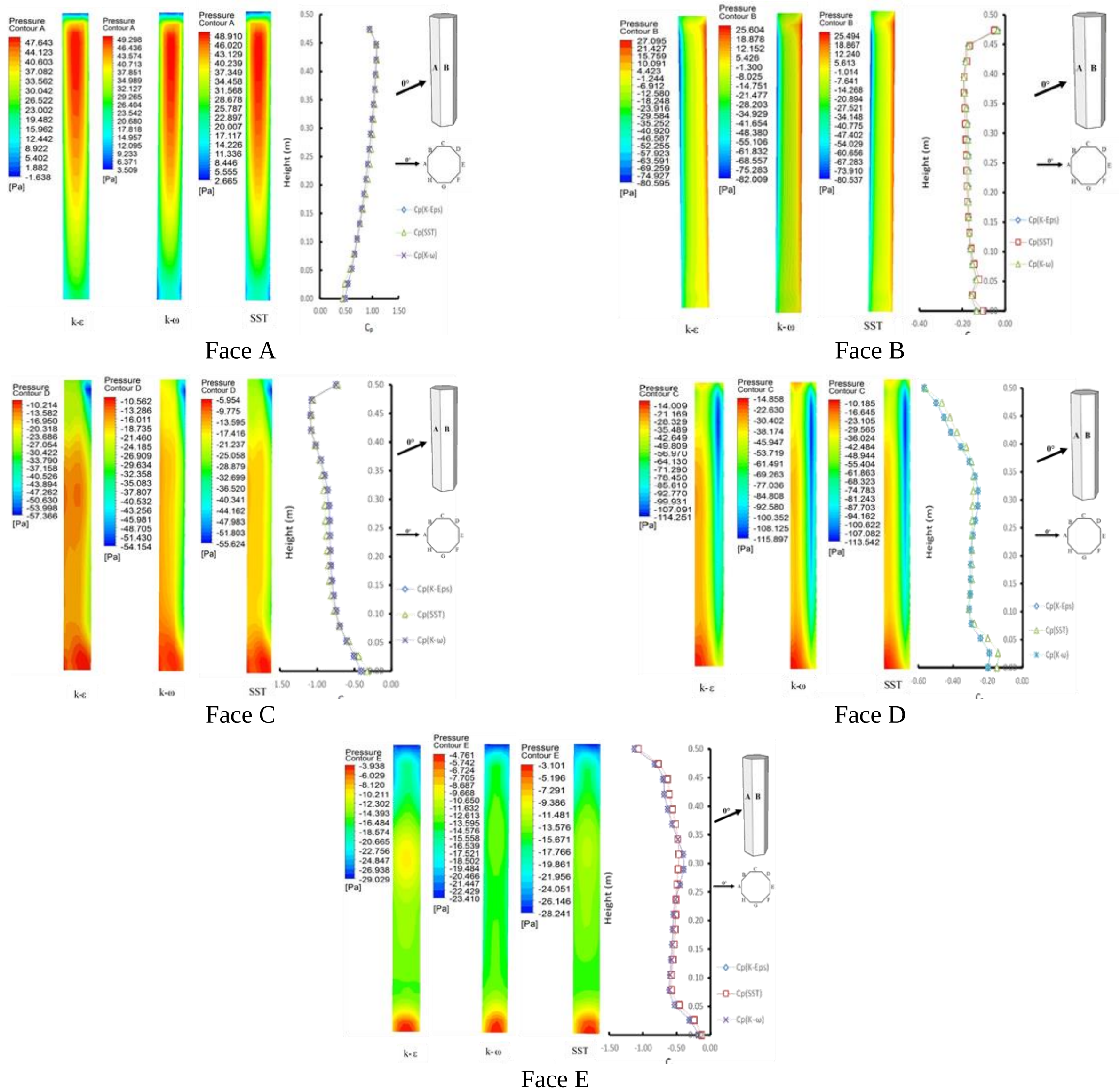

Fig. 7 Comparison of pressure coefficient along the vertical centreline and pressure contours on five faces for different methods

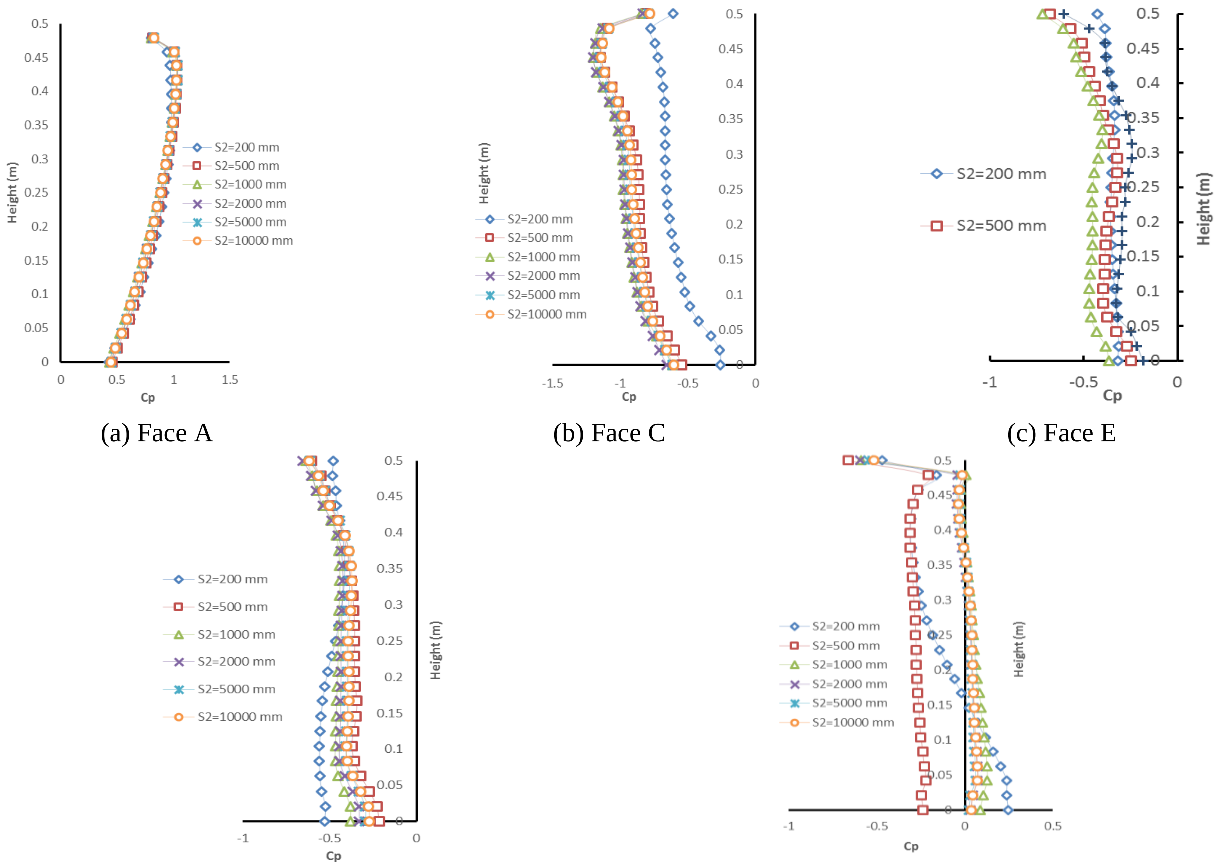

(a) Face A (b) Face C (c) Face E

(d) Face F (e) Face H

Fig. 8 Comparison of variation of pressure coefficient along vertical centreline if S_3 = 200 mm for different faces

In this case the values from ANSYS CFX does not quite match with AS/NZS-1170.2 (2011) as there is no definite aspect ratio for the octagon plan shaped building is mentioned. But it shows very little deviation from the other cases.

Wind flow pattern and pressure variation

The flow pattern for this case is shown in Fig. 6. The main features observed are summarized as follows. The flow pattern is symmetrical due to the plan shape being symmetrical. The wind flow separates after colliding with the windward face i.e., Face A so it will have positive pressure values with negative values only at the edges due to flow separation. The pressure distribution is also symmetrical about the vertical centreline. The inclined windward faces i.e., Face B and Face H will have positive pressure near the edge of Face A and gradually be negative away from Face A. The side faces C and G has negative pressure due to side wash. Face D, E and F have negative pressure due to formation of vortices. Face E has a semi-circular zone at the bottom and an elliptical zone at the middle, where the negative values of the pressure are relatively lower.

Comparison between different numerical models

A comparative study is done between pressure coefficients resulted from three different analytical models (k-ε, SST and k-ω). Fig. 7 shows the comparison of pressure coefficient along the vertical centreline as well as pressure contours on five faces for three different methods. It can be seen that the Height vs. C_p plots for K-**ε** and K-**ω** are identical and there is only small difference in SST.
The pressure coefficients for different faces of the octagon plan shaped building for various numerical models are shown in Table 4. The symmetric surfaces have more or less same C_p for all the methods. The maximum deviation is 2.2% between faces D and F by k-ω model. The deviation in C_p between any two models for different faces are also negligible for most of the cases, the maximum deviation being 11.1% for face D between k-ε and k-ω model.

6.1.2 Interference condition

In this case the building setup is subjected to wind flow at the wind incidence angle 0°. In this condition five cases are discussed as follows

Case I (S_1=200 mm, S_3=200 mm)

In this case S_1 and S_3 remains constant whereas S_2

Table 4 Face average values of pressure coefficients on different faces of the octagon plan shaped building

Location	Mean C_p for 0° wind angle		
	k-ε	**SST**	**k-ω**
Face A	0.780	0.795	0.81
Face B	-0.293	-0.290	-0.285
Face C	-0.946	-1.01	-1.03
Face D	-0.369	-0.402	-0.410
Face E	-0.584	-0.594	-0.622
Face F	-0.365	-0.396	-0.401
Face G	-0.942	-1.02	-1.03
Face H	-0.289	-0.285	-0.284

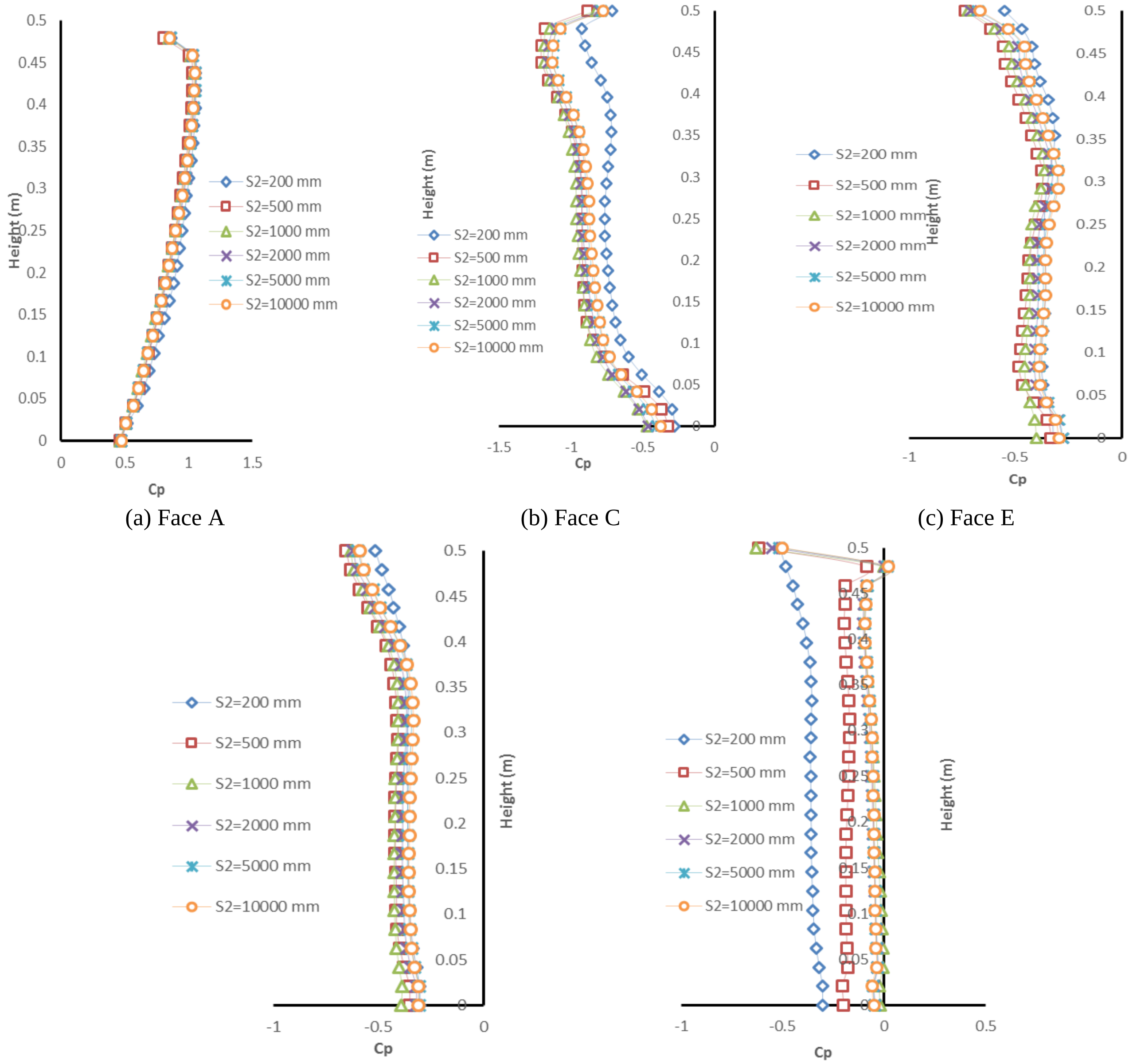

(a) Face A (b) Face C (c) Face E

(d) Face F (e) Face H

Fig. 9 Comparison of variation of pressure coefficient along vertical centreline if S_3 = 300 mm for different faces

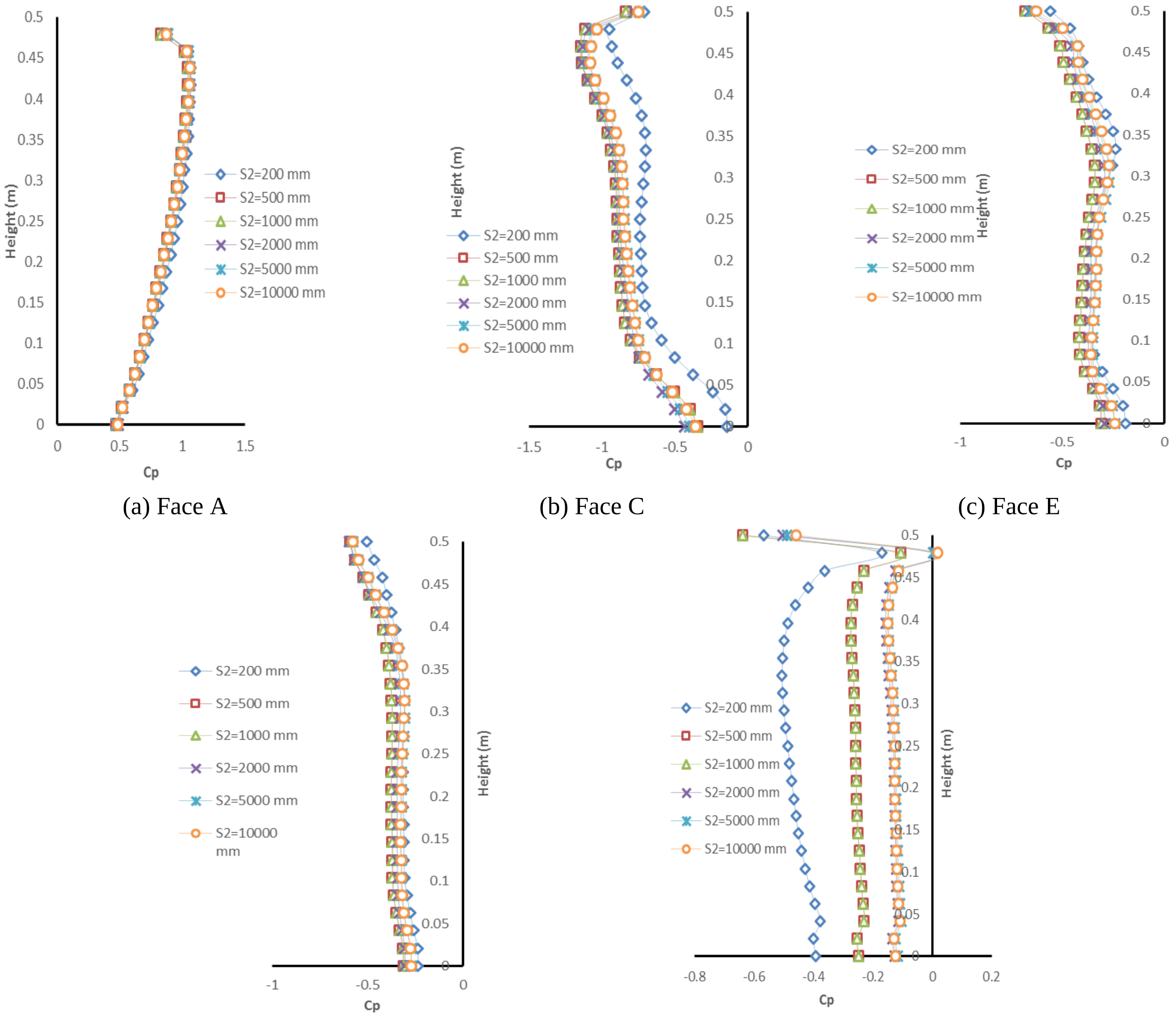

(a) Face A (b) Face C (c) Face E

(d) Face F (e) Face H

Fig. 10 Comparison of variation of pressure coefficient along vertical centreline if S_3 = 500 mm for different faces

varies from 200 mm to 10000 mm. The variation of pressure coefficient on the faces A, C, E, F and H along the vertical centreline against different S_2 values are shown in Figs. 8(a)-8(e). In this case no definite increase or decrease pattern can be observed for any face. Especially for face H the variation of pressure coefficient is arbitrary due to the combined effect of shielding effect due to third interfering building and channelling effect due to buildings 1 and 2 (Fig. 4).

Case II (S_1=200 mm, S_3=300 mm)

For Case II S_1 and S_3 remains constant whereas S_2 varies from 200 mm to 10000 mm. The variation of pressure coefficient on the faces A, C, E, F and H along the vertical centreline against different S_2 values are shown in Figs. 9(a)-9(e). The variation of pressure coefficients in different faces in this case are similar to that of Case I except for face H. The height vs. C_p curve does not show any positive value in this case contrary to the case I.

Case III (S_1=200 mm, S_3=500 mm)

Here S_1 and S_3 remains constant whereas S_2 varies from 200 mm to 10000 mm. The variation of pressure coefficient on the faces A, C, E, F and H along the vertical centreline against different S_2 values are shown in Figs. 10(a)-10(e). In this case for face H a definite decrease in C_p variation is noted with the increase of S_2. This is because as S_2 increases the shielding effect of building 3 becomes prevalent than the channelling effect due to buildings 1 and 2 (Fig. 4).

Case IV (S_1=200 mm, S_3=750 mm)

For Case IV S_1 and S_3 remains constant whereas S_2 varies from 200 mm to 10000 mm. The variation of pressure coefficient on the faces A, C, E, F and H along the vertical centreline against different S_2 values are shown in Figs. 11(a)-11(e). Variation of C_p in this case for different faces are similar to that of case III. It is noted that no

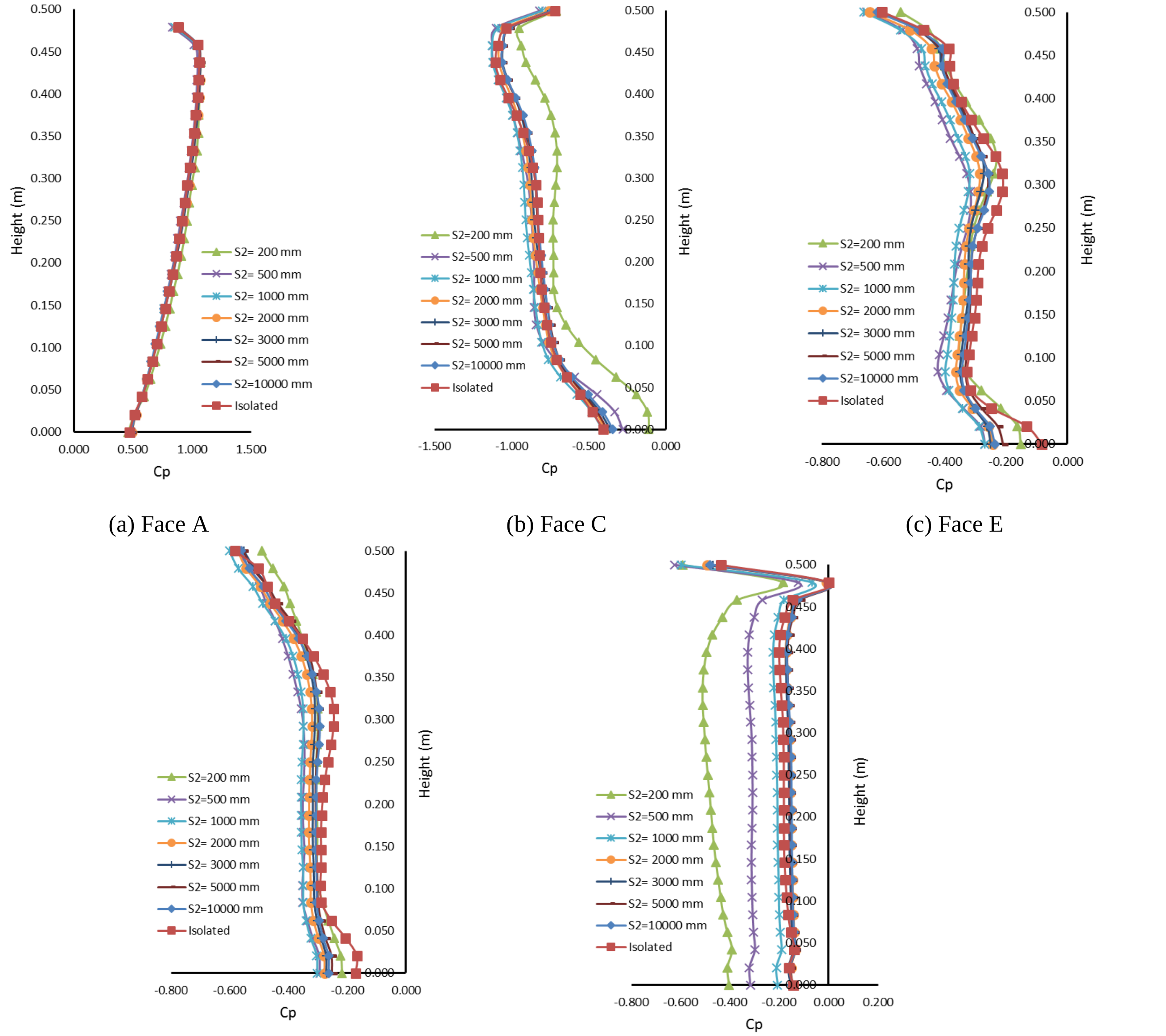

(a) Face A (b) Face C (c) Face E

(d) Face F (e) Face H

Fig. 11 Comparison of variation of pressure coefficient along vertical centreline if S_3 = 750 mm for different faces

condition coincides with the isolated condition for most of the faces.

<u>*Case IV (S_1=200 mm, S_3=1000 mm)*</u>

In this case S_1 and S_3 remains constant whereas S_2 varies from 200 mm to 10000 mm. The variation of pressure coefficient on the faces A, C, E, F and H along the vertical centreline against different S_2 values are shown in Figs. 12(a)-12(e). In this case we can observe that the C_p variation for the isolated case more or less coincides with that of case S_1=200 mm, S_2=10000 mm and S_3=1000 mm for all the faces. This case can be considered an optimum case with respect to interference condition.

6.1.3 Interference factor

Interfering factor for any point is given by Eq. (21)

$$IF_p = \frac{Pressure\ at\ any\ point\ in\ interfering\ condition}{Pressure\ at\ that\ point\ in\ isolated\ condition} \quad (21)$$

Interference factor thus found can be used to plot Interference Factor contour for each face of the octagon plan shaped building. Interference factor for above mentioned case for faces B, C, E, F and H are shown in Fig. 13. These IF contours can be used to understand the local interference effect for different faces of the octagon plan shaped building. Where the contour lines are concentrated on different faces, it can be deduced that a rapid change in IF occurs there. On faces B and H contour lines are concentrated near small zones, hence the IF variation is maximum in these regions. In case of faces C and F numerous contour lines are observed, so IF changes very rapidly throughout these faces.

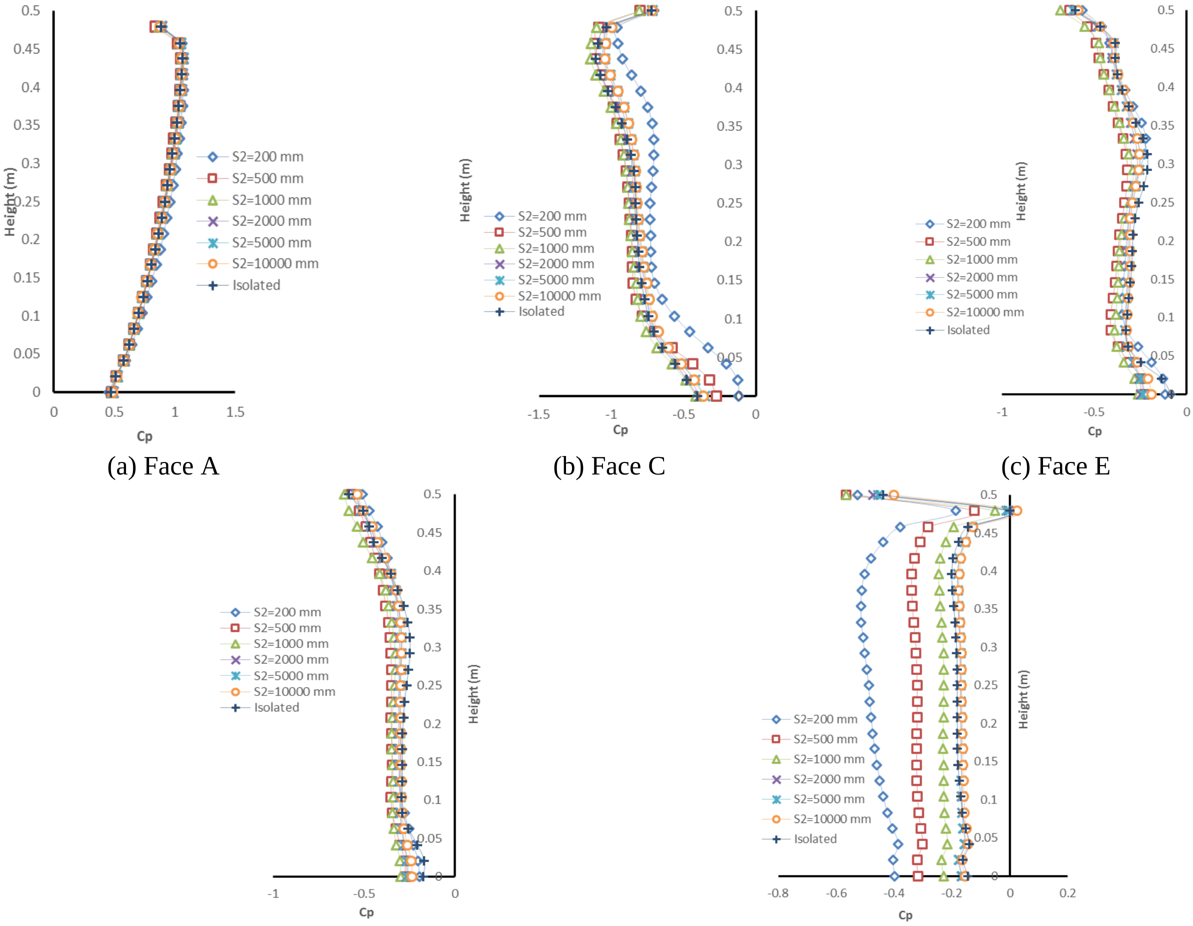

(a) Face A (b) Face C (c) Face E

(d) Face F (e) Face H

Fig. 12 Comparison of variation of pressure coefficient along vertical centreline if S_3 = 1000 mm for different faces

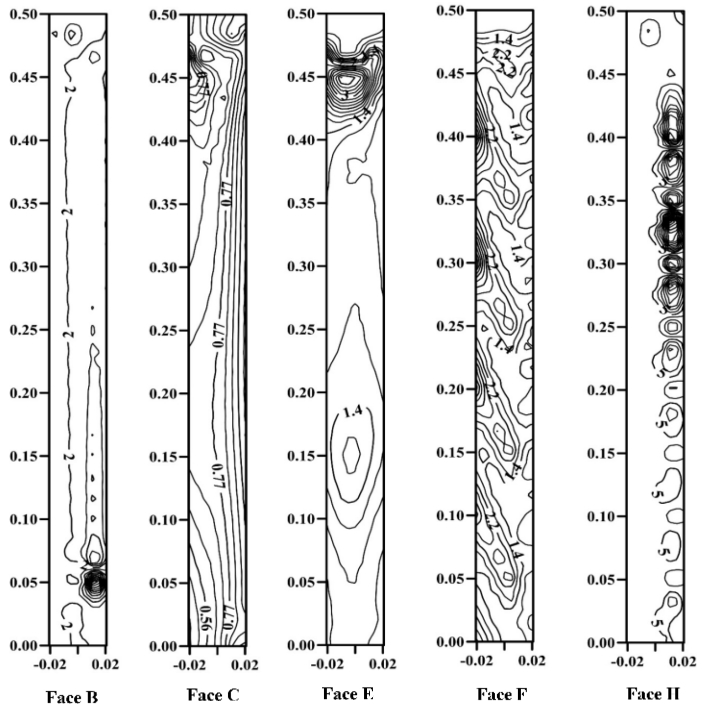

Fig. 13 Interference Factor contour for different faces of the Octagon plan shaped building

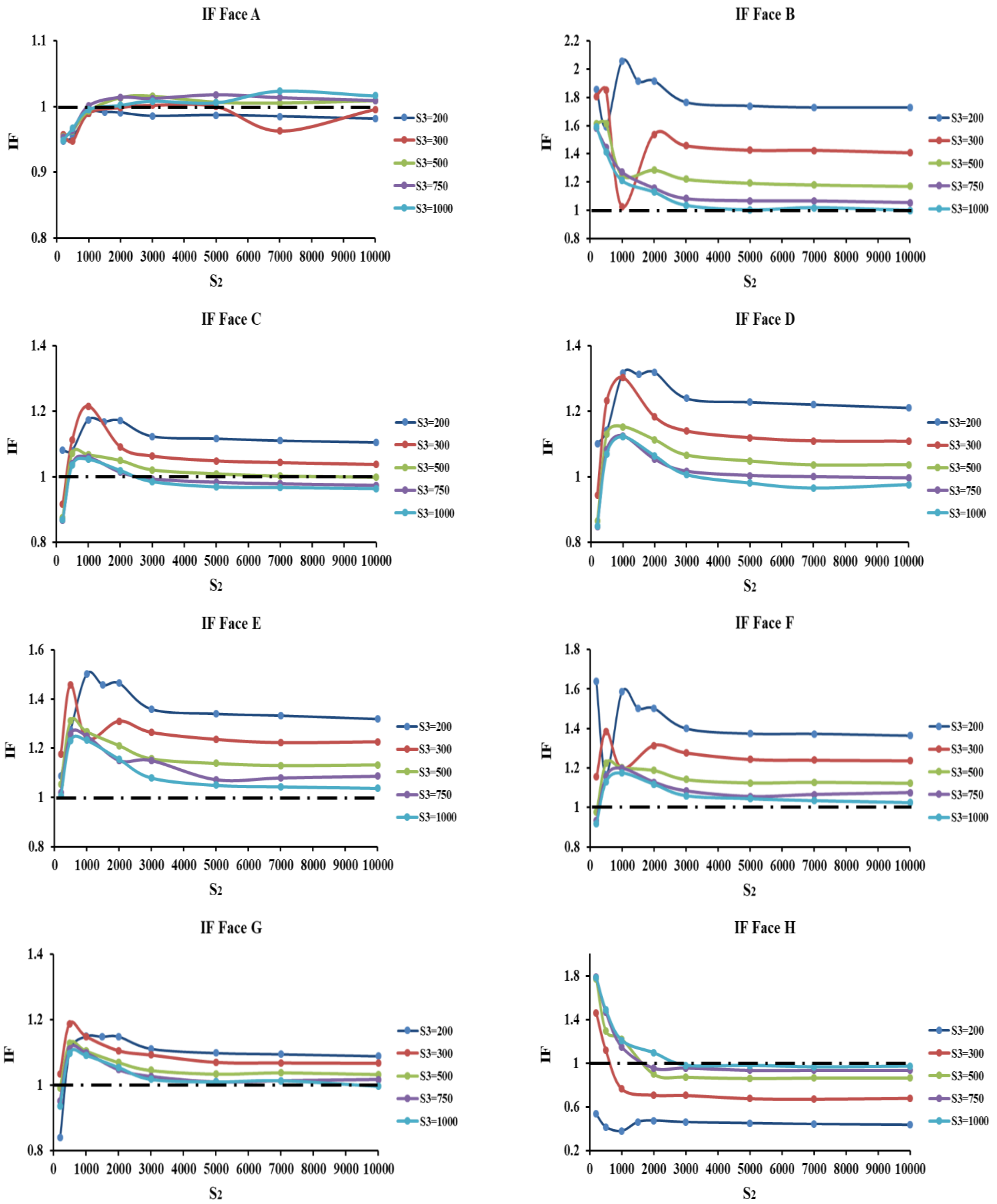

Fig. 14 Comparison of IF on different faces for varying distance between the buildings for S_1=200 mm

Mean interference factor

Interference effects are presented in the form of non-dimensional Interference Factors (IF) that represent the aerodynamic forces on an octagon plan shaped study building with interference from adjacent three square plan shaped buildings. Mean IF is given by the formula in Eq. (22)

$$IF_{Face} = \frac{Mean\ Pressure\ on\ a\ face\ in\ interfering\ condition}{Mean\ Pressure\ on\ a\ face\ in\ isolated\ condition} \quad (22)$$

Table 5 Response surface models for different faces

Face	Response Surface Models	R^2
A	$IF_A = 0.9248 - 0.0315 \times S_1 + 0.0376 \times S_2 + 0.132 \times S_3 + 0.0019 \times S_1^2 - 0.0026 \times S_2^2 - 0.1605 \times S_3^2$	0.978
B	$IF_B = 1.953 - 0.1187 \times S_1 - 0.0551 \times S_2 + 0.2631 \times S_3 + 0.0068 \times S_1^2 - 0.0054 \times S_2^2 - 1.1919 \times S_3^2$	0.919
C	$IF_C = 1.2664 - 0.0159 \times S_1 + 0.0701 \times S_2 - 1.1294 \times S_3 + 0.0006 \times S_1^2 - 0.0064 \times S_2^2 + 0.7662 \times S_3^2$	0.974
D	$IF_D = 1.5097 - 0.0105 \times S_1 + 0.0909 \times S_2 - 1.8754 \times S_3 + 0.0001 \times S_1^2 - 0.0087 \times S_2^2 + 1.3073 \times S_3^2$	0.981
E	$IF_E = 1.6543 - 0.0379 \times S_1 + 0.0719 \times S_2 - 1.6413 \times S_3 + 0.0019 \times S_1^2 - 0.0069 \times S_2^2 + 1.0022 \times S_3^2$	0.946
F	$IF_F = 1.862 - 0.0308 \times S_1 + 0.0973 \times S_2 - 2.5911 \times S_3 + 0.0012 \times S_1^2 - 0.0096 \times S_2^2 + 1.7537 \times S_3^2$	0.959
G	$IF_G = 1.1697 - 0.032 \times S_1 + 0.0505 \times S_2 - 0.5341 \times S_3 + 0.0018 \times S_1^2 - 0.0044 \times S_2^2 + 0.2889 \times S_3^2$	0.987
H	$IF_H = -0.7992 - 0.1776 \times S_1 - 0.245 \times S_2 + 8.6787 \times S_3 + 0.0131 \times S_1^2 - 0.0262 \times S_2^2 - 7.1126 \times S_3^2$	0.949

Here S_1, S_2 and S_3 are in meter.

If C_p be the face average value of pressure coefficient for a particular face in isolated condition then the same for any particular interfering condition is given by Eq. (23).

$$C_{p,interfering} = \mathrm{IF}_{\mathrm{Face}} * C_p \tag{23}$$

The comparison between the mean IFs with varying distance between study building and interfering buildings are shown graphically in Fig. 14. The variation of IF on face A for different interference cases is negligible. For faces B, C, D, E, F and G the IF is greater than unity for most of the cases. This is due to the channelling effect of interfering buildings 1 and 3. For face H however the IFs are less than unity for most of the cases. This is due to shielding effect of interfering building 3. IF approaches unity when S_3 is increased for all faces except face A. The IF generally assumes lesser values, when S_2 is less than 1000 mm on all faces except faces B and H, due to shielding effect of the interfering buildings 1 and 2. For faces B and H the general trend is that the IF values are higher when S_2 is less than 1000 mm.

6.2 Interference condition by RSM and optimization approach

The IFs from different interfering conditions are predicted with the help of the RSM. 13 random cases are analysed by ANSYS CFX and used as the input data for constructing the metamodels using MATLAB R2016a as per the process described in Fig. 5. These predictions are arranged in form of expressions for IFs at each face in terms of S_1, S_2 and S_3. The Response Surface Models for the IF of eight faces are shown in Table 5. The coefficient of determination (R^2) values as defined hereunder is also indicated in the table.

$$R^2 = \frac{\sum_{l=1}^{t}\left(\widehat{Y_l} - \overline{Y_l}\right)^2}{\sum_{l=1}^{t}\left(Y_l - \overline{Y_l}\right)^2} \tag{24}$$

Where Y_l, $\widehat{Y_l}$, and $\overline{Y_l}$ are the actual response obtained by the CFD, the RSM predicted response and the mean of the actual response respectively. 't' is the total number of best points (considered here as 30) to arrive at the R^2 values. It can be observed that the R^2 values are more than 0.9 indicating a good fit. However, it is expected that an adaptive metamodelling technique based on Kriging or Moving Least Square method would produce more accurate models with R^2 values very close to unity. This is under consideration at this stage.

The comparison of IFs between CFD analysis and Response Surface Model are shown in Fig. 15. The case S_1=200 mm, S_2=10000 mm and S_3=1000 mm is an optimum condition case, i.e. IFs for all the faces are unity. In this case the maximum deviation between ANSYS and Response Surface method is 7.1%. For S_1=200 mm, S_2=1000 mm and S_3=200 mm, it is a high interference condition case. In this case the maximum deviation between ANSYS and Response Surface method is 8.3%. So, for both the cases deviation is within acceptable limit (10% considered here). Thus, it can be stated that the Response Surface Model is a very good representation of the interference condition of the current building setup.

6.2.1 Proposed RSM based optimization scheme

Once the RSM is validated, the optimization is executed by the SQP (Sequential Quadratic Programming). The optimization is executed by two schemes:

i. Without uncertainty effect by Eq. (13)
ii. Incorporating uncertainty effect by Eq. (20)

The objective function in the optimization is plotted against S_1 and S_2 and the resultant response surface is depicted in Fig. 16.

By plotting the outputs obtained from optimization of the Response Surface Models an Interference Zone can be constructed. Whenever there is presence of an interfering building outside of this zone no interference effect on the study building is observed. After incorporation of the uncertainty approach in the optimization of the response surface model some definite locations of the interfering buildings can be found where the effect of interference of this buildings on the study building is minimal even after considering the uncertain nature of wind. The original interference zone which is developed without considering uncertainty along with the expanded zone after incorporation of uncertainty approach is depicted in Fig. 17.

Computational efficiency achieved by using RSM based optimization approach is shown in Table 6. It can be observed that the proposed RSM based approach can complete the entire process by only seven days. Also, it

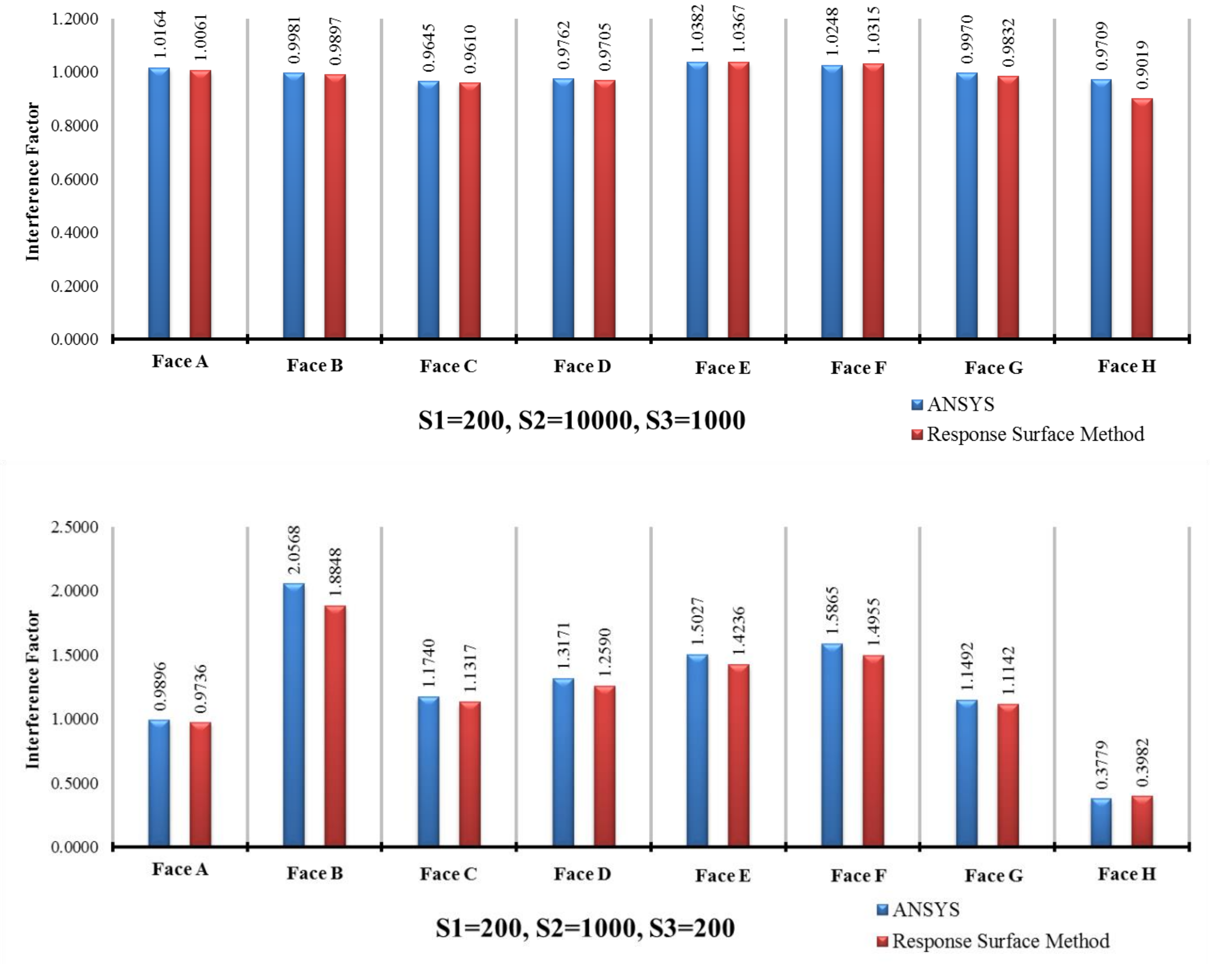

Fig. 15 Comparison between IFs from ANSYS CFX and RSM

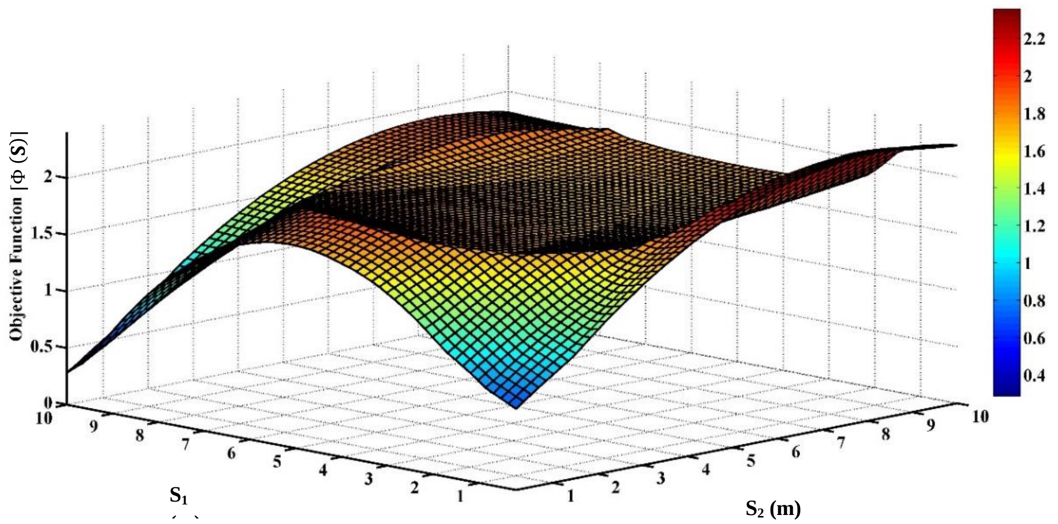

Fig. 16 Response surface of objective function for optimization against S_1 and S_2

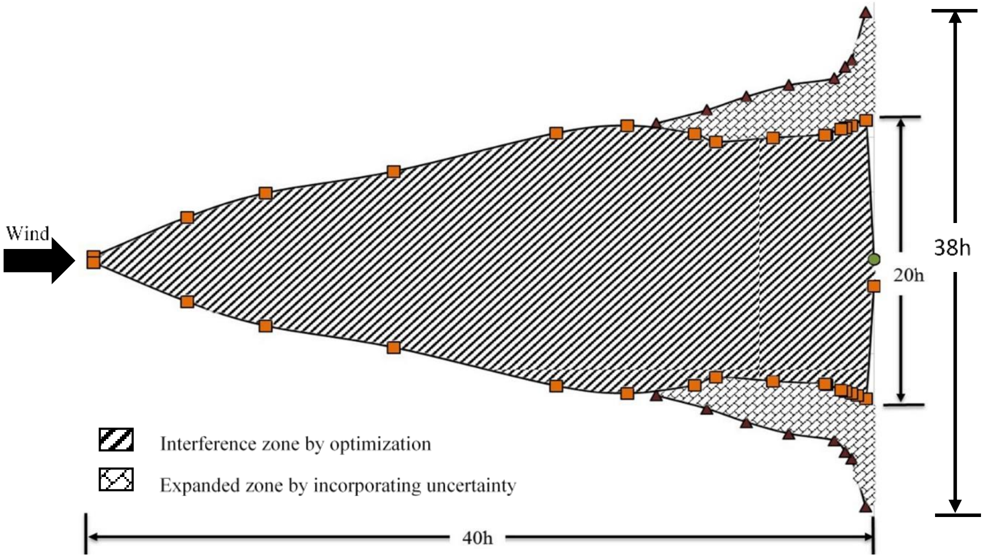

Fig. 17 Interference Zone and its expansion with the application of uncertainty approach

Table 6 Approximate time taken to yield the Interference Zone

Method Adopted	By CFD analysis	By proposed RSM based optimization approach
Time Taken	500 Days	7 Days

uses only 13 runs of CFD. Whereas by direct CFD analysis the same interference zone can be obtained by around 500 days, since many random CFD run is to be undertaken. Moreover, the calculation of gradients and incorporation of uncertainty cannot be done by the direct CFD analysis unless the help of RSM is taken.

7. Conclusions

The conclusions that can be drawn from the results of the current study are as follows

- It is evident from the numerical simulation by ANSYS CFX that the responses on the octagon plan shaped building in isolated condition is symmetrical in nature. K-**ε,** SST and K-**ω** has produced similar pressure distribution on all the faces of octagon plan shaped building in isolated condition.
- From the five cases of interference conditions discussed, it can be seen that the variation of pressure distribution follows a predictable pattern except some cases. The variation becomes less predictable when the interfering buildings are positioned closely to the study building. Especially face H shows unusual variation in pressure distribution when the across wind interfering building is near the study building ($S_3 \leq 500$ mm).
- The Interference Factor contour can be a powerful tool for analysing the local interference on any face.
- The mean IFs for any intermediate case other than that mentioned in the study can be found out from graphical plot as depicted in Fig. 14.
- The Response Surface Model (Table 5) can be used to find out the IFs for any values of S_1, S_2 and S_3 for the current building setup. The model is constructed using only 13 analysed cases as input. If this was analysed only by CFD analysis or wind tunnel experiment minimum 600 iterations have to be performed. By using the Response Surface modelling, the tedious and time-consuming job has been simplified by leaps and bounds. Thus, the proposed approach is not only accurate but also computationally efficient.
- The development of the Interference Zone is a very important target of the current study. The size of the interference zone is 40h upstream from the study building and 20h across wind spanning in both sides of the study building (Fig. 17). The width of the zone increases to 38h across wind near the study building due to introduction of uncertainty approach. It is to be noted that the downstream interference effect is not considered here.

References

ASCE/SEI 7-10 (2010), Minimum Design Loads for buildings and other structures.

AS-NZS 1170-2 (2011), (English): Structural design actions - Part 2: Wind actions.

Bhandari, A., Datta, G. and Bhattacharjya, S. (2018), “Efficient wind fragility analysis of RC high rise building through metamodelling”, *Wind Struct.*, **27**(3), 199-211.

Chen, X., Fan, J. and Bian, X. (2017), “Structural robust optimization design based on convex model”, *Results in Physics*, **7**, 3068-3077.

Dalui, S.K. (2008), Wind effects on tall buildings with peculiar shapes, Doctoral dissertation. Indian Institute of Technology Roorkee, Roorkee, India. Retrieved from http://shodhbhagirathi.iitr.ac.in:8081/xmlui/handle/123456789/1633

Ganguli, R. (2002), "Optimum design of a helicopter rotor for low vibration using aeroelastic analysis and response surface methods", *J. Sound Vib.*, **258**(2), 327-344.

Hang, J., Li, Y. and Sandberg, M. (2011), "Experimental and numerical studies of flows through and within high-rise building arrays and their link to ventilation strategy", *J. Wind Eng. Ind. Aerod.*, **99**(10), 1036-1055.

Hui, Y., Tamura, Y. and Yang, Q. (2017), "Analysis of interference effects on torsional moment between two high-rise buildings based on pressure and flow field measurement", *J. Wind Eng. Ind. Aerod.*, **164**, 54-68.

Hui, Y., Tamura, Y. and Yoshida, A. (2012), "Mutual interference effects between two high-rise building models with different shapes on local peak pressure coefficients", *J. Wind Eng. Ind. Aerod.*, **104-106**, 98-108.

Hui, Y., Tamura, Y., Yoshida, A. and Kikuchi, H. (2013), "Pressure and flow field investigation of interference effects on external pressures between high-rise buildings", *J. Wind Eng. Ind. Aerod.*, **115**, 150-161.

Hui, Y., Yoshida, A. and Tamura, Y. (2013), "Interference effects between two rectangular-section high-rise buildings on local peak pressure coefficients", *J. Fluid. Struct.*, **37**, 120-133.

IS 875-Part 3 (2015), Indian Standard code of practice for design loads (other than earthquake) for building and structures, bureau of Indian standard, New Delhi.

Lam, K.M., Leung, M.Y.H. and Zhao, J.G. (2008), "Interference effects on wind loading of a row of closely spaced tall buildings", *J. Wind Eng. Ind. Aerod.*, **96**(5), 562-583.

Lam, K.M., Zhao, J.G. and Leung, M.Y.H. (2011), "Wind-induced loading and dynamic responses of a row of tall buildings under strong interference", *J. Wind Eng. Ind. Aerod.*, **99**(5), 573-583.

Li, J.Y., Li, R., Gao, Y. and Huang, J. (2010), "Aerodynamic optimization of wind turbine airfoils using response surface techniques", *Proceedings of the Institution of Mechanical Engineers, Part A: Journal of Power and Energy*, **224**(6), 827-838.

Lo, Y.L., Kim, Y.C. and Li, Y.C. (2016), "Downstream interference effect of high-rise buildings under turbulent boundary layer flow", *J. Wind Eng. Ind. Aerod.*, **159**, 19-35.

Lo, Y.L., Kim, Y.C. and Yoshida, A. (2017), "Effects of aerodynamic modification mechanisms on interference from neighboring buildings", *J. Wind Eng. Ind. Aerod.*, **168**, 271-287.

Mara, T.G., Terry, B.K., Ho, T.C.E. and Isyumov, N. (2014), "Aerodynamic and peak response interference factors for an upstream square building of identical height", *J. Wind Eng. Ind. Aerod.*, **133**, 200-210.

Myers, R.H., Montgomery, D.C. and Cook, C.M.A. (2009), *Response surface methodology process and product optimization using designed experiments*, John Wiley and Sons, Inc.

Spence, S.M.J. and Gioffrè, M. (2012), "Large scale reliability-based design optimization of wind excited tall buildings", *Probab. Eng. Mech.*, **28**, 206-215.

Venanzi, I. and Materazzi, A.L. (2013), "Robust optimization of a hybrid control system for wind-exposed tall buildings with uncertain mass distribution", *Smart Struct. Syst.*, **12**(6), 641-659.

Wang, F., Tamura, Y. and Yoshida, A. (2014), "Interference effects of a neighboring building on wind loads on scaffolding", *J. Wind Eng. Ind. Aerod.*, **125**, 1-12.

Wu, Y., Huang, J., Yan, G., Yan, X. and Lü, J. (2016), "Optimization of isolation structure under wind load excitation and experimental study of the wind resistant bearing", *J. Shanghai Jiaotong Univ. (Science)*, **21**(6), 719-728.

Yan, B. and Li, Q.S. (2016), "Wind tunnel study of interference effects between twin super-tall buildings with aerodynamic modifications", *J. Wind Eng. Ind. Aerod.*, **156**, 129-145.

Yu, X.F., Xie, Z.N., Wang, X. and Cai, B. (2016), "Interference effects between two high-rise buildings on wind-induced torsion", *J. Wind Eng. Ind. Aerod.*, **159**, 123-133.

Yu, X.F., Xie, Z.N., Zhu, J.B. and Gu, M. (2015), "Interference effects on wind pressure distribution between two high-rise buildings", *J. Wind Eng. Ind. Aerod.*, **142**, 188-197.

Zhang, A. and Gu, M. (2008), "Wind tunnel tests and numerical simulations of wind pressures on buildings in staggered arrangement", *J. Wind Eng. Ind. Aerod.*, **96**(10-11), 2067-2079.

Zu, G.B. and Lam, K.M. (2018), "Across-wind excitation mechanism for interference of twin tall buildings in staggered arrangement", *J. Wind Eng. Ind. Aerod.*, **177**, 167-185.

AD